

Article

# Flow Separation Control in a Curved Diffuser with Rigid Traveling Wave Wall and Its Mechanism

Weiye Lu \*, Guoping Huang, Jinchun Wang and Yuxuan Yang

College of Energy and Power Engineering, Nanjing University of Aeronautics and Astronautics, Nanjing 210016, China; hgp@nuaa.edu.cn (G.H.); jinchunwang@nuaa.edu.cn (J.W.); yyx@nuaa.edu.cn (Y.Y.)

\* Correspondence: lwy\_651@nuaa.edu.cn

Received: 2 December 2018; Accepted: 4 January 2019; Published: 8 January 2019



**Abstract:** Traveling wave wall is a useful method to suppress flow separation. However, the interaction between the traveling wave wall and unsteady separation flow is complex, which causes difficulty in discovering the corresponding mechanism. To reveal the mechanism of traveling wave wall control, numerical simulation of a separated curved diffuser using rigid traveling wave wall flow control is performed, which shows some unique characteristics. Then, a nonlinear simplified model is used to explain this phenomenon in flow control in consideration of nonlinear dynamics and order of degree. Flow field data from the numerical simulation are further analyzed using fast Fourier transform analysis, linear stability theory of free shear layers, and the nonlinear simplified model to reveal the control mechanism of traveling wave wall.

**Keywords:** flow control; traveling wave wall; nonlinear model; mechanism study

## 1. Introduction

Flow separations often occur in fluid machinery and result in large flow loss and energy consumption, which need to be avoided as much as possible using flow control methods. The traveling wave wall, which originated from the field of bionics, is an effective unsteady flow control method. The application of this method is expected to increase in the future with the development of flexible intelligent material technology.

The photos shot by Hertel [1] in 1966 showed that, when dolphins swim in and leap out of the water in high speed, their skin surface forms a wave, which may relate to their outstanding maneuverability. In other words, dolphins' skin folds may reduce the swimming resistance, which is the bionic origin of the traveling wave wall control method. Choi [2] experimentally used the flexible moving wall for flow control and found that the turbulent drag can be decreased to approximately 7%.

The numerical study of Wu C. J. [3,4] showed that the traveling wave wall forms a stable fluid roller bearing (FRB) effect with proper wavelength, amplitude, and wave phase velocity. Furthermore, the traveling wave wall can suppress large separation and vortex shedding from airfoils at large angles of attack or stationary cylinders. Moreover, finite length transverse traveling wave (TTW) of several wavelengths can produce a stable FRB effect even under strong adverse pressure gradient.

Wu J. M. [5] theoretically explained drag reduction of traveling wave wall through 2D infinite TTW. The results showed that, for a given waveform and amplitude, a critical phase velocity of the wave exists and extinguishes the time-averaged shear near the wall. As a result, the flow resistance decreases to zero. Wu J. Z. [6] verified this prediction by numerical simulation. The numerical study of Yang [7] indicated that the FRB effect of the traveling wave can establish a series of small-scale vortices that can separate the main stream from the near-wall shear flow and result in drag reduction of friction and pressure resistances.

Wu Q. Y. [8] studied the effect of traveling wave wall on unsteady separated flow and vortex-induced vibration of a cylinder by numerical simulation. The results showed that the original shedding vortex frequency is locked to the frequency of the traveling wave when the velocity ratio (phase velocity of wave over inflow velocity) is larger than 1. The drag of the cylinder is decreased to 99.6% when the velocity ratio equals 2. The shedding vortex is completely inhibited when the velocity ratio equals 3.

Chen [9] experimentally studied traveling wave wall control on the surface of a cylinder to verify the forced perturbation mechanism. When the phase velocity of the traveling wave is higher than the critical value, the vortex shedding frequency can be locked to the frequency of traveling wave. He discovered the resonant perturbation mechanism for the first time. Specifically, when the frequency of traveling wave is close to that of natural vortex shedding, the control effect is strong; however, the speed of traveling wave and energy consumed are low (the speed ratio is nearly 0.03).

In summary, traveling wave wall is an unsteady flow control method and serves as an external excitation to flow separations. However, vortical structures of unsteady separated flow fields and the interaction between unsteady external and separation flows are complex. Some theories of traveling wave wall have been proposed, such as the FRB effect and forced perturbation and resonant perturbation mechanisms. However, the control mechanism, which can be obtained from numerous data of the unsteady flow fields, is still unclear. Traveling wave wall relies on flexible intelligent material technology, which is still not mature and feasible to engineering applications. Thus, a rigid traveling wave wall that is compact, low energy consuming, and practical is proposed in this study to probe the mechanism of traveling wave wall control.

A curved diffuser with rigid traveling wave wall flow control is numerically simulated to obtain the unique characteristics and complex flow field data of the traveling wave wall control. A complex phenomenon does not always mean a complex mechanism. Previous results of unsteady flow control showed that the shedding vortex is more orderly with proper unsteady periodic control than without control [10]. In other words, traveling wave control may be connected to chaos control and reflected by a nonlinear simplified model. On the basis of our previously established nonlinear simplified model [11], we attempt to interpret the mechanism of the traveling wave control. A deep and precise mechanism can be obtained from a large quantity of information due to high complexity of unsteady separation flows [12,13]. Thus, fast Fourier transform (FFT) for frequency spectrum analysis is used combined with the simplified model to analyze the mechanism deeply buried in flow field data. Although two-dimensional flows are focused on by the works with regard to traveling wave wall at this stage, it is worth mentioning that secondary flows or three-dimensional effects play an important role in turbulent boundary layers [14] and flow controls [15]. So, traveling wave walls designed for three-dimensional flows will be paid attention to in the future.

## 2. Numerical Simulation of Flow Control in a Curved Diffuser Using Traveling Wave Wall

### 2.1. Diffuser and Its Numerical Method

To obtain the characteristics of traveling wave wall control, the unsteady flow separation in a curved diffuser with rigid traveling wave wall control is numerically simulated. The adopted diffuser and rigid wave wall are illustrated in Figure 1a.

The diffuser is two-dimensional and it is formed by the pressure and suction surfaces of a stator blade and corresponding inlet and outlet sections. The main parameters of this diffuser are listed in Table 1. The traveling wave wall is the combination of a cylinder and a sinusoidal curve, which is described by the equation  $r = 11 - \sin(5\theta)$  (mm) in polar coordinates (as illustrated in Figure 1c). The minimum clearance between the traveling wave wall and its circular container is 0.3 mm. The rotation radius, wavelength, and wave amplitude are fixed, whereas the rotational speed or phase velocity of the traveling wave can be adjusted. Detailed parameters of the traveling wave wall are also shown in Table 1.

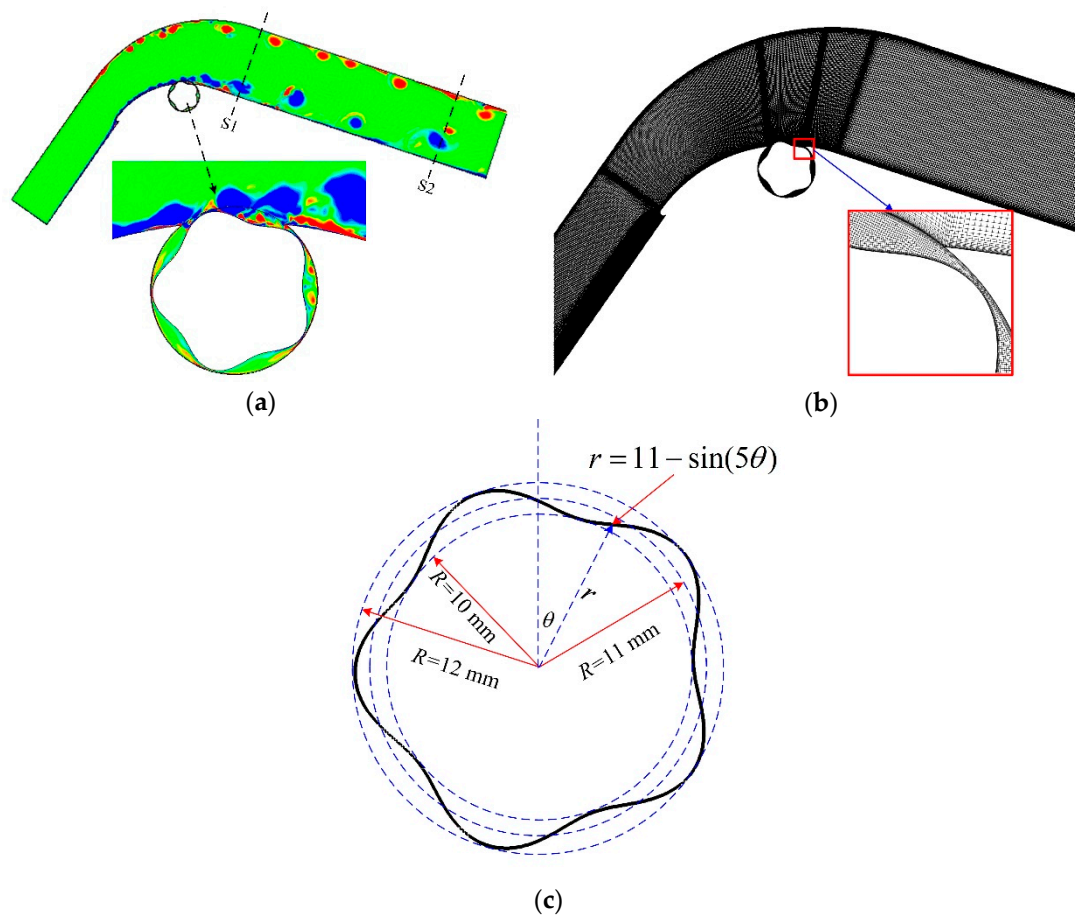


**Figure 1.** Adopted diffuser, mesh for numerical simulation and rigid traveling wave wall control: (a) geometry of the diffuser and rigid traveling wave wall; (b) the mesh for numerical simulation; (c) the geometry of the traveling wave wall.

**Table 1.** Main parameters of the adopted diffuser and traveling wave wall.

Part	Parameter	Value
Diffuser	Inlet Mach number	0.1
	Inlet attack angle/degree	9
	Chord length of the blade/mm	80
	Inlet width/mm	34.3
	Outlet width/mm	55
Traveling wave	Wavelength/mm	13.8
	Wave amplitude/mm	1
	Rotation radius/mm	11
	Number of full waves	5

Large eddy simulation (LES) is used to analyze the separation phenomenon in consideration of the influence of small vortices added by Smagorinsky–Lilly sub-grid model. And ANSYS Fluent software is used for the numerical simulation. To validate the numerical method, we compare the numerical and experimental results of the static pressure coefficient on the suction surface of the curved diffuser without any flow control (shown in Figure 2a where  $c$  is the chord length of the blade). The numerical result basically agrees with that of the experiment. The grid-independent study is performed as shown in Figure 2b. When the grid number is higher than  $9 \times 10^4$ , the total pressure loss is nearly invariant, and the simulated performance is independent of the grid. Considering both computational accuracy and economy, the grid number used is about  $1 \times 10^5$ . The mesh grids (illustrated in Figure 1b) near

walls and leading and trailing edges are densified to satisfy the demand of LES that  $y^+ \approx 1$  near walls. Clearly speaking, the near-wall grid scale is set as 0.01 mm, and it is about 25 times the Kolmogorov scale length (the Kolmogorov scale length  $\eta \approx \nu/v_0 \approx (1.5 \times 10^{-5} \text{ m}^2/\text{s})/(35 \text{ m/s}) \approx 4 \times 10^{-4} \text{ mm}$ ). In addition, a combination of structural and unstructured meshes is used to guarantee grid quality in the diffuser and traveling wave regions. Boundary conditions of the inlet and outlet are set to make the inlet Mach number approximately 0.1 (the Reynolds number defined by the length of blade chord is  $1.81 \times 10^5$ ), whereas the surface between traveling wave wall and main flow in the diffuser is treated as rotor–stator interface. Dual-time stepping is used to solve the unsteady process with the physical time step of  $10^{-5} \text{ s}$ . For traveling wave wall, we are concerned with the fully-developed state (rather than the transient state) when the traveling wave fully interacts with the unsteady flow field and the influence of the initial field is negligible. So, when the outlet mass flow rate is quasi-periodic, the flow field is considered to be fully-developed, and only a period ( $10^4$  physical time steps) of fully-developed unsteady flow field is analyzed.

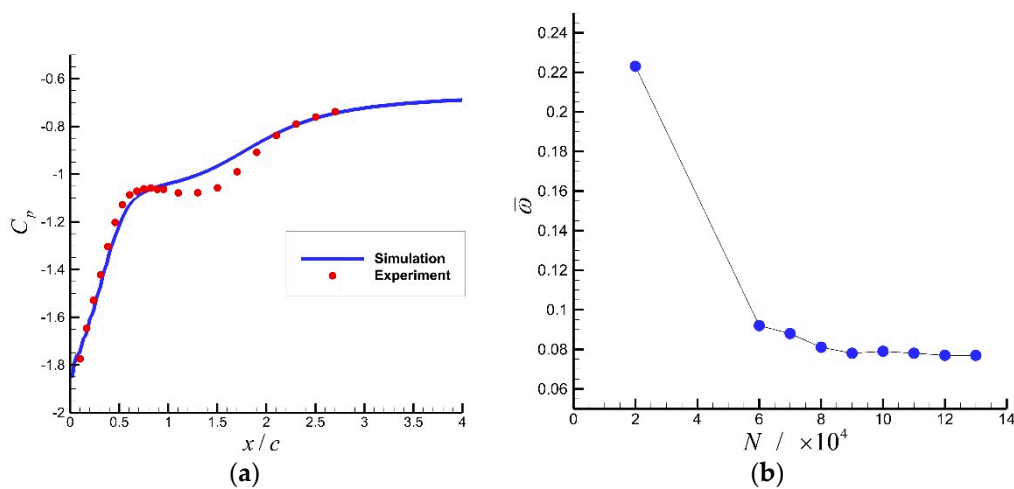


**Figure 2.** Validation and grid-independent study of the numerical method: (a) simulated and experimental static pressure coefficient  $C_p$  on the suction surface of the curved diffuser without any flow control; (b) total pressure loss coefficient  $\bar{w}$  versus grid number  $N$ .

## 2.2. Dimensionless Parameters and Evaluation Indexes of Control Effect

Traveling wave wall flow control involves important dimensionless parameters, such as dimensionless phase velocity of the traveling wave and frequency. Dimensionless phase velocity is defined as

$$\tilde{V} = \frac{v_{TWW}}{v_0}, \quad (1)$$

where  $v_{TWW}$  is the phase velocity of the traveling wave wall and equals the average rotational speed of the wall surface.  $v_0$  is the average velocity of the diffuser inlet and serve as a characteristic velocity.

When phase velocity of the traveling wave differs, the effect of unsteady external excitation on the main flow also differs, especially its frequency. Phase velocity equals wavelength times frequency and is described as

$$v_{TWW} = \lambda f_{TWW}, \quad (2)$$

where  $\lambda$  is the wavelength of the traveling wave and  $f_{TWW}$  is the frequency of the traveling wave.

When the main frequency of shedding vortex of diffuser without flow control is used as the characteristic frequency, dimensionless frequency can be defined as

$$\tilde{f} = \frac{v_{TWW}}{\lambda f_0}, \quad (3)$$

where  $f_0$  is the main frequency of shedding vortex.

The total pressure loss coefficient is used with the commonly used definition as follows:

$$\bar{\omega} = \frac{P_0^* - P_1^*}{\frac{1}{2}\rho_0 v_0^2}, \quad (4)$$

where  $P_0^*$  is the total pressure at the diffuser inlet,  $P_1^*$  is the total pressure at the diffuser outlet, and  $\rho_0$  is the density of air and is considered constant because the Mach number is smaller than 0.3. To reflect the control effect, a relative total pressure loss coefficient is introduced and defined as

$$\bar{\omega}_r = \frac{\bar{\omega}_c - \bar{\omega}}{\bar{\omega}} = \frac{P_1^* - P_c^*}{P_0^* - P_1^*}, \quad (5)$$

where  $P_c^*$  is the total pressure at the diffuser outlet with flow control. However, given that additional energy is introduced into the flow field by the traveling wave wall, the total and relative total pressure loss coefficients cannot always reflect the flow control effect or energy saving. Thus, energy efficiency is introduced and defined by us. The energy equation has a simplified form as follows:

$$\frac{P_0}{\rho_0} + \frac{v_0^2}{2} + H = \frac{P_1}{\rho_0} + \frac{v_1^2}{2} + h_\omega, \quad (6)$$

where  $P_0$  is the static pressure at the diffuser inlet,  $P_1$  is the static pressure at the diffuser outlet,  $v_1$  is the average velocity at the diffuser outlet,  $H$  is the energy added to the flow per unit mass flow rate by the traveling wave wall, and  $h_\omega$  is the mechanical energy loss per unit mass flow rate. From Equation (6), we derive the following equation:

$$\dot{m} \frac{P_0^* - P_1^*}{\rho_0} = \dot{m}(h_\omega - H), \quad (7)$$

where  $\dot{m}$  stands for the mass flow rate. For the diffuser without flow control ( $H = 0$ ), we have

$$\dot{m} \frac{P_0^* - P_1^*}{\rho_0} = \dot{m}h_\omega. \quad (8)$$

For the diffuser with flow control, we obtain

$$\dot{m} \frac{P_0^* - P_c^*}{\rho_0} = \dot{m}(h_{\omega c} - H) = \dot{m}h_{\omega c} - \omega_{TWW}T_{TWW}, \quad (9)$$

where  $T_{TWW}$  is the time-averaged torque of the traveling wave wall due to pressure and viscous drags and  $\omega_{TWW}$  is the angular velocity of the traveling wave wall ( $\omega_{TWW} = 2\pi f_{TWW}/5$ ). Energy efficiency is defined as the mechanical energy saved due to flow control divided by energy consumed due to flow control, which can be deduced using Equations (8) and (9) as

$$\varepsilon = \frac{h_\omega - h_{\omega c}}{H} = \frac{\dot{m}(P_c^* - P_1^*)}{\rho_0 \omega_{TWW} T_{TWW}} - 1. \quad (10)$$

The definition of energy efficiency indicates that the flow control is economical only when  $\varepsilon > 1$ ; otherwise, the flow control may be effective but energy consuming.

### 2.3. Results and Analysis of the Numerical Simulation

Figure 3a shows the change in relative total pressure loss coefficient as the dimensionless phase velocity or frequency increases. Dimensionless frequency is proportional to dimensionless phase velocity when wavelength is fixed. Thus, they share the same x-axis. As shown in Figure 3a,

the relative total pressure loss coefficient generally decreases as the dimensionless phase velocity increases. However, some minimum points lie on the curve when  $\tilde{V} \approx 0.14$ ,  $\tilde{V} \approx 0.2$ , and  $\tilde{V} \approx 0.3$ , or the corresponding  $\tilde{f} \approx 1$ ,  $\tilde{f} \approx 1.5$ , and  $\tilde{f} \approx 2.3$ , which signifies better control effect than the adjacent points. These discrete minimum points reflect the unsteady control property of traveling wave wall. Figure 3b indicates that, as dimensionless phase velocity increases, energy consumed by traveling wave wall increases gradually first and then rapidly. The trend is similar to a parabola.

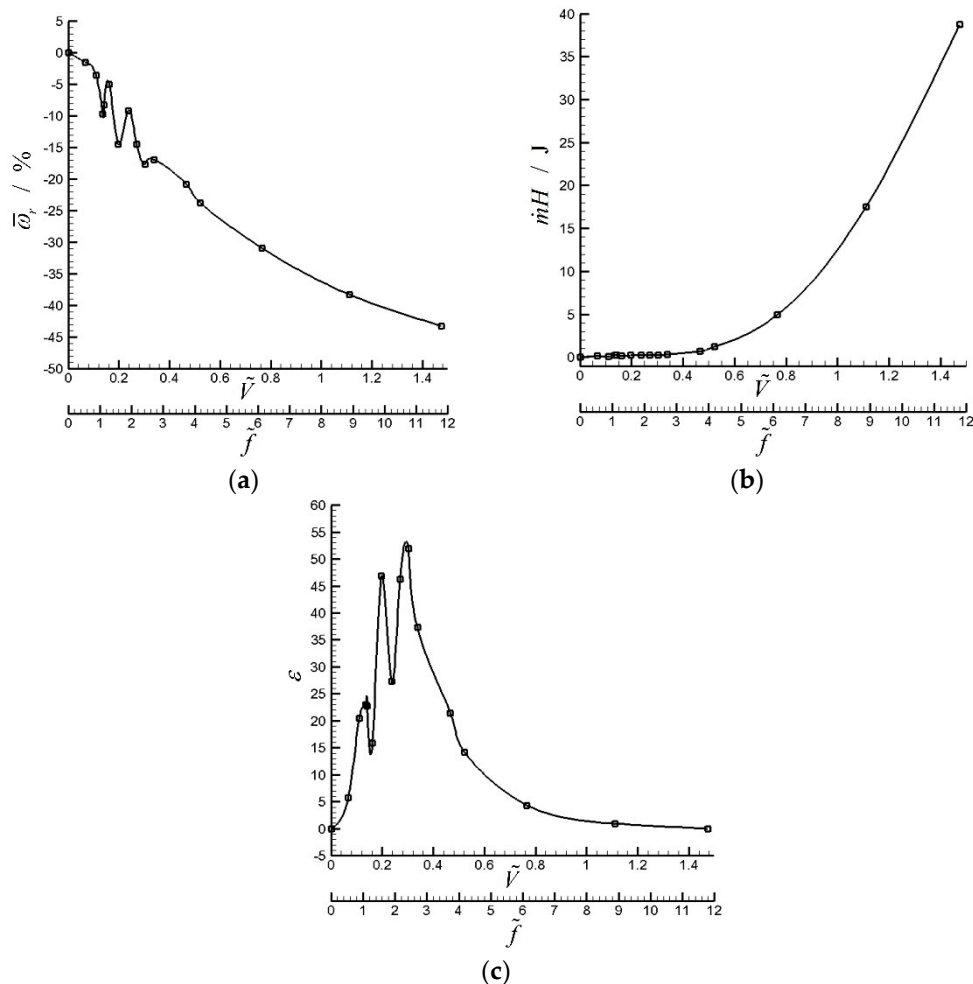


**Figure 3.** Simulation results: (a) relative total pressure loss coefficient  $\bar{\omega}_r$  versus dimensionless phase velocity  $\tilde{V}$  or frequency  $\tilde{f}$ ; (b) energy consumed by the traveling wave wall  $mH$  versus dimensionless phase velocity  $\tilde{V}$  or frequency  $\tilde{f}$ ; (c) energy efficiency  $\varepsilon$  versus dimensionless phase velocity  $\tilde{V}$  or frequency  $\tilde{f}$ .

Considering the monotonous trend of relative total pressure loss coefficient and energy consumed by traveling wave wall, energy efficiency as the new parameter is used to further reflect the control effect, as shown in Figure 3c. Figure 3c indicates that energy efficiency increases first and then decreases. Some maximum points on the curve correspond to those in Figure 3a. Therefore, when  $\tilde{f} \approx 1$ ,  $\tilde{f} \approx 1.5$ , and  $\tilde{f} \approx 2.3$ , the traveling wave wall not only has good control effect but also uses less energy. However, when the dimensionless phase velocity is more than 1.1, energy efficiency is less than 1. In other words, the traveling wave wall is energy consuming under this case. The reason is that, when the speed of traveling wave wall is sufficiently fast, part of traveling wave wall that is covered by the diffuser and has no effect on the flow control consumes much energy, which results in waste of energy.

The numerical results reveal unique and peculiar characteristics of traveling wave wall control, especially in the discrete windows of good control effect around  $\tilde{f} \approx 1$ ,  $\tilde{f} \approx 1.5$ , and  $\tilde{f} \approx 2.3$ , similar to

the resonant perturbation mechanism mentioned before. We use a nonlinear simplified model to interpret this phenomenon in flow control. As a result, a possible relationship between unsteady flow and chaos controls in nonlinear dynamics can be obtained.

### 3. Nonlinear Simplified Model and Its Analysis

#### 3.1. Duffing-Based Model for Traveling Wave Control

In accordance with [11], we establish a Duffing-based model (simplified cross-direction motion model, SCDM model for short) based on 2D incompressible N-S equation and Stuart vortex row model. The SCDM model is shown as

$$\frac{d^2y}{dt^2} = \varepsilon\omega_0^2y - \frac{4\varepsilon\omega_0^2}{r_0^2}y^3 - K_0\frac{dy}{dt} + A_0\sin(\omega_0t), \quad (11)$$

where  $y$  is the cross motion of fluid particle;  $t$  denotes time;  $\omega_0$  and  $r_0$  are the characteristic frequency and radius of the Stuart vortex, respectively;  $K_0$  is the equivalent damping coefficient due to fluid viscosity and small-scale vortex viscosity;  $\varepsilon$  is a constant that equals 0.818 from the deduction; and  $A_0$  represents the amplitude of Kelvin–Helmholtz (K–H) unstable wave [16]. Equation (11) is a forced Duffing equation with negative linear and positive cubic stiffness [17]. The model describes the cross motion (indicated by the  $y$  coordinate) of a certain fluid particle in the Stuart vortex row around its unstable boundary [11]. The model is used to approximately describe the rolled-up large-scale vortical structures due to K–H instability in the free shear layer [18].

External excitation such as traveling wave wall must be added to Equation (11), which describes flow separation without control. The traveling wave wall may have two effects on the flow field. One is to change the natural frequency of the field, and the other is to produce an additional unsteady excitation to the field. The unstable flow field such as a separated flow has natural or dominant frequency caused by quasi-periodically shedding vortices, and this frequency may be changed by flow controls. Traveling wave wall, as an unsteady flow control, can also generate external unsteady excitation and interact with vortices in the flow field, such as resonant perturbation. The effect of traveling wave wall on the nonlinear simplified model is modeled corresponding to the two functions.

On the basis of the Stuart vortex row, Equation (11) approximately describes an unsteady flow field without flow control, and the characteristic frequency and scale of separation vortices are  $\omega_0$  and  $r_0$ , respectively. However, with flow control of traveling wave wall, the characteristic frequency and scale of separation vortices may be changed to  $\omega$  ( $\omega = k\omega_0$ , and  $k$  is a coefficient) and  $r$ . Similarly,  $K_0$  and  $A_0$  in Equation (11) may be changed to  $K$  and  $A$ . Thus, the equation used to describe the unsteady flow field with separation vortices of the frequency and scale denoted as  $\omega$  and  $r$  is shown as follows:

$$\frac{d^2y}{dt^2} = \varepsilon\omega^2y - \frac{4\varepsilon\omega^2}{r^2}y^3 - K\frac{dy}{dt} + A\sin(\omega t). \quad (12)$$

In other unsteady flow control studies, researchers have already found that the best periodic excitation location for separation flow control is near the separation point [10,14]. This condition indicates that flow instability is essentially sensitive to outside disturbance near the separation point [19]. Therefore, external unsteady excitation of the traveling wave wall can be modeled similar to K–H waves.

To imitate the modeling of K–H wave, external unsteady excitation of traveling wave wall is modeled as  $A_e \cos(\omega_e t)$ . Then, it is added to Equation (12), where  $\omega_e$  is the frequency of traveling wave wall and  $A_e$  is its intensity. Thus, the simplified model with external excitation such as traveling wave wall can be written as

$$\frac{d^2y}{dt^2} = \varepsilon\omega^2y - \frac{4\varepsilon\omega^2}{r^2}y^3 - K\frac{dy}{dt} + A\sin(\omega t) + A_e\sin(\omega_e t). \quad (13)$$

To make this equation non-dimensional, the parameters in Equation (13) are replaced as follows:  $y/r \rightarrow y$ ,  $t\sqrt{\varepsilon}\omega \rightarrow t$ ,  $K/\sqrt{\varepsilon}\omega \rightarrow K$ ,  $A/\varepsilon\omega^2r \rightarrow A$ ,  $A_e/\varepsilon\omega^2r \rightarrow A_e$ ,  $k\omega_0 \rightarrow \omega$ , and  $\omega_e/\omega_0 \rightarrow \omega_e$ . As a result, the non-dimensional expression of Equation (13) (only this form is used in the subsequent parts) can be written as (using  $1/\sqrt{\varepsilon} \approx 1.1$ )

$$\frac{d^2y}{dt^2} = y - 4y^3 - K\frac{dy}{dt} + A \sin(1.1t) + A_e \sin(1.1\frac{\omega_e}{k}t). \quad (14)$$

Only five parameters are independent in this non-dimensional expression. Among these parameters, non-dimensional damping coefficient  $K$  and non-dimensional amplitude of dominant K–H wave  $A$  depend on the characteristic of the unsteady flow field. Besides, non-dimensional intensity of excitation  $A_e$ , non-dimensional frequency of excitation  $\omega_e$ , and coefficient  $k$  depend on the external excitation such as traveling wave wall. In particular,  $K$  depends on Reynolds number of the flow field, and  $A$  depends on the intensity of the K–H wave of flow particles. To simplify the analysis, the two non-dimensional parameters are assumed to be invariant with the change in  $\omega_e$  because the flow states are assumed to be similar except for different frequencies and scale of vortices. Parallel to the traveling wave wall control,  $\omega_e$  plays the same role as  $\tilde{f}$ ,  $A_e$  describes the intensity of excitation (considered the same with different values of  $\omega_e$ ), and  $k$  describes the change in natural frequency due to traveling wave wall. In particular,  $k$  is a function of  $\omega_e$ , that is,  $k = k(\omega_e)$ . Thus, the simplified model with external excitation such as vibration wall is completely prepared.

When  $A_e = 0$ , no excitation is added to the flow field. When  $A_e > 0$  and  $\omega_e = k$ , the most unstable frequency (dominant frequency) of K–H wave is enhanced and resonant perturbation mechanism may occur according to [9]. When  $\omega_e \neq k$ , the non-dominating K–H wave enhances and coexists with the dominant one.

### 3.2. Characteristics of the Nonlinear Simplified Model without and with Traveling Wave Wall Control

The maximum Lyapunov exponent (MLE), as a criterion to evaluate the control effect, is introduced to describe the degree of order in the simplified model. In nonlinear dynamic systems, evolutionary trajectories may be sensitive to the initial values, which can result in chaos or “butterfly effect”. MLE is a parameter that describes the tendency of evolutionary trajectories with adjacent initial values. When the MLE is less than zero, evolutionary trajectories converge, which indicates that the motion is stable. However, when the MLE is more than zero, evolutionary trajectories diverge, which indicates that the motion is unstable or chaotic. Thus, MLE is a criterion used to judge whether the system is chaotic. In this study, the computational method of MLE is based on that proposed by Benettin in [20].

First, the model without flow control, that is, Equation (14) with  $A_e = 0$ , is studied. This equation is known as Duffing equation [17]. Then, a set of parameters is used to obtain solutions of Equation (14), such as in a real flow separation [11]. In this case, the set of parameters is tentatively selected as  $K = 0.154$  and  $A = 0.18$ .

The corresponding time–displacement and velocity–displacement phase diagrams are shown in Figure 4a,b. The two figures show that the fluid element lies in the unstable region. Moreover, its trajectory in the velocity–displacement phase diagram changes from one strange attractor to another, which brings difficulty in forecasting the tendency. This condition is chaotic [21] and accords with the chaotic phenomena in the actual flow separation qualitatively. However, chaotic phenomena do not correspond to randomness and irregularity because coherent structures still exist in chaotic dynamic systems. As observed from the frequency spectrum by FFT in Figure 4c, the non-dimensional dominant frequency (defined as the frequency of FFT multiplied by  $2\pi/1.1$ ) of this dynamic system is 1. This result indicates that periodicity still exists in the seemingly chaotic fluctuation phenomenon, and nonlinearity generates wide band frequency spectrum. As a result, the frequencies of clutters differ from the dominant frequency of K–H wave (of which the non-dimensional frequency equals 1).

The MLE is calculated as 0.175, which is larger than zero and implies that the dynamic system is in a chaotic condition.

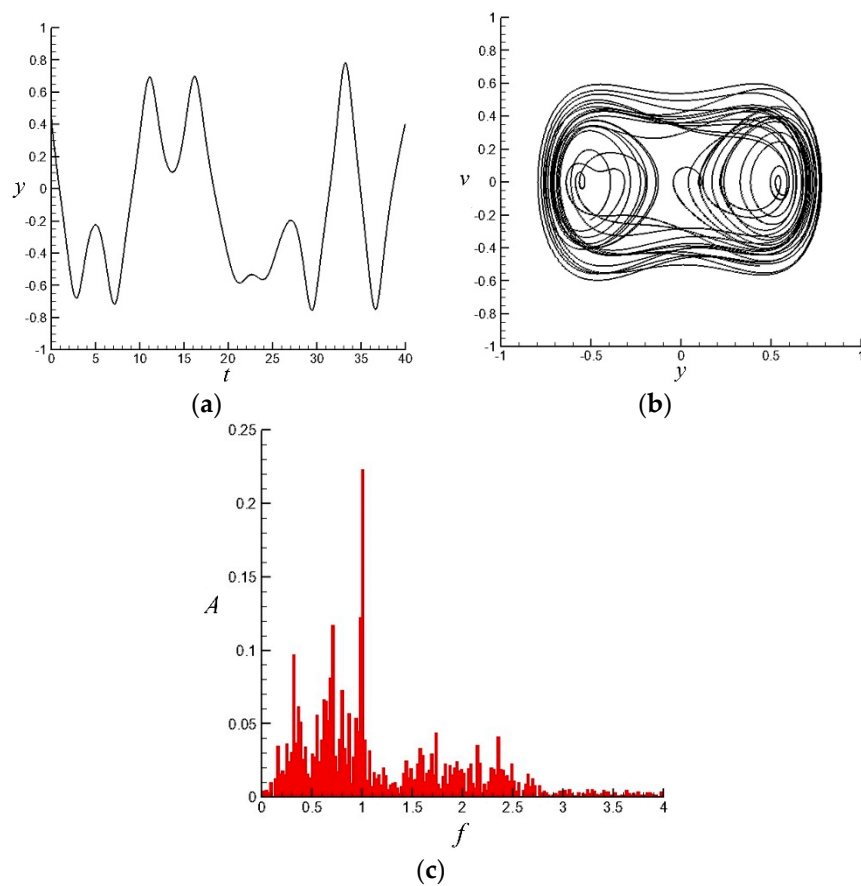


**Figure 4.** Response of the model without control (all variables are nondimensional): (a) Time–displacement ( $y - t$ ) diagram; (b) Velocity–displacement phase ( $v - y$ ) diagram; (c) FFT of displacement ( $A - f$ ).

When  $\omega_e$  is small, the traveling wave wall cannot change the natural frequency of the flow field ( $v_{TWW}$  is also small). Thus,  $k(\omega_e)$  equals 1 when  $\omega_e$  is small. However, a very large  $\omega_e$  serves as a smooth cylinder felt by the flow field and will also barely affect the natural frequency. As a result,  $k(\omega_e \rightarrow \infty) \rightarrow const$ . In the simplified model,  $k(\omega_e)$  is first given, as shown in Figure 5, to determine if it can generate similar results to those in Figure 3, and  $A_e = 0.24$  in Equation (14). The MLE is then calculated with increased dimensionless frequency  $\omega_e$ , which is also shown in Figure 3. The trend of MLE is similar to that in Figure 3. Specifically, when the values of  $\omega_e$  are around 1, 1.6, and 2.1, MLE considerably decreases and even tends to below zero. Low MLE indicates that the fluctuation characteristics of the fluid element will be less chaotic and even change from chaotic states to periodic states. This result verifies the resonant perturbation mechanism because, when the frequency of external excitation equals the natural frequency of the flow field (or some integer multiple, which will be discussed in the following passage), the flow field will be orderly and the flow loss will be considerably decreased compared with those under the controls by adjacent frequencies.

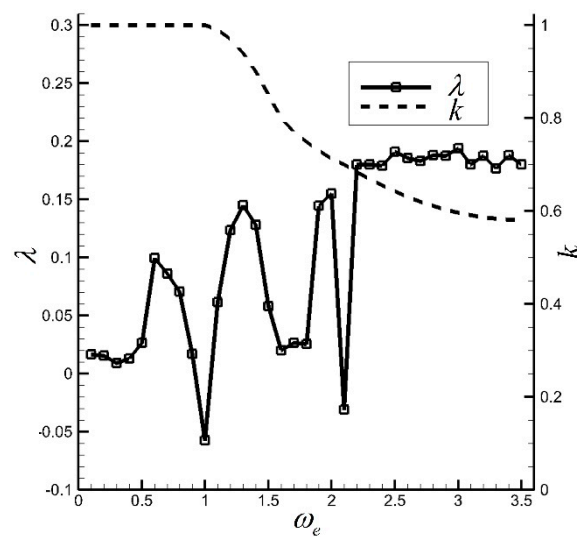


**Figure 5.** MLE ( $\lambda$ ) of the simplified model with traveling wave wall control.

Time–displacement and velocity–displacement phase diagrams are shown in Figure 6a,b when the reduced frequency is valid, where  $\tilde{f}$  is 1. From the analysis of these figures, the mechanism of good control effect when dimensionless frequency equals some unique frequencies can be determined. With valid external periodic excitation, the motion of fluid element is entirely orderly and periodic. This result is also reflected by MLE ( $-0.05$ ). FFT of displacement with valid excitation is shown in Figure 6c. Compared with those in Figure 4c, valid excitation eliminates many clutters and the frequency spectrum is only dominated by the main system frequency and three times of it (due to the cubic nonlinear term).

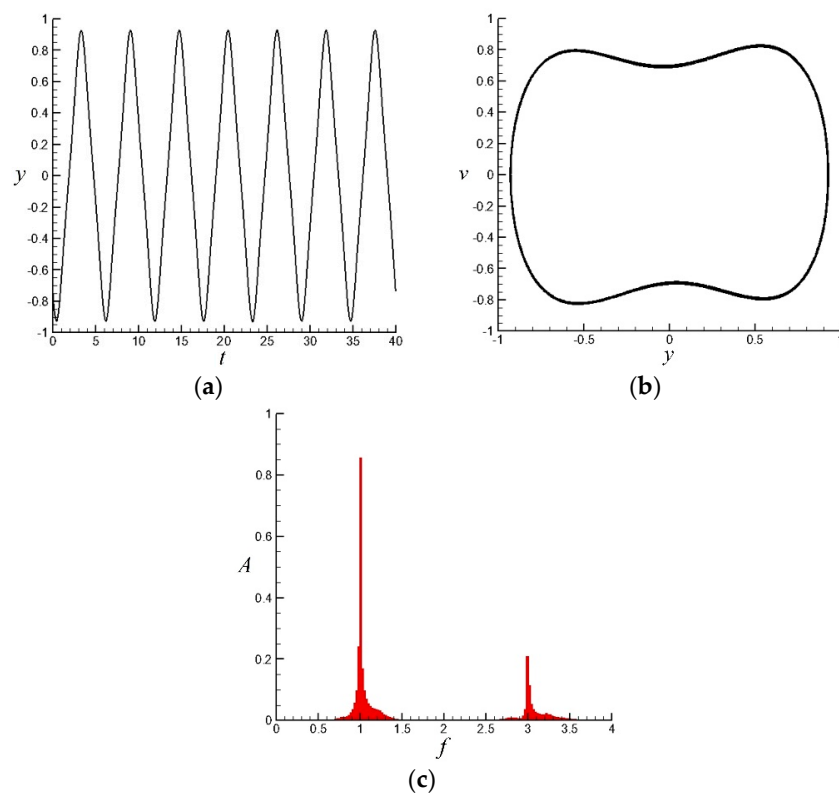


**Figure 6.** Response of the model with effective control ( $\tilde{f} = 1$ ): (a) Time–displacement ( $y - t$ ) diagram; (b) Velocity–displacement phase ( $v - y$ ) diagram; (c) FFT of displacement ( $A - f$ ).

In this section, the resonant perturbation mechanism is partially explained by the simplified model with external excitation such as traveling wave wall. Valid excitation can exhibit resonance with the main frequency of the flow field and make it orderly. The natural frequency of the model is changed, and this modification successfully explains the phenomenon found in the numerical simulation. To further verify this deduction, FFT will be used to deal with the data from the numerical simulation, and additional detailed results will be presented in the subsequent section.

#### 4. Mechanism Analysis of Flow Control Using Traveling Wave Wall

##### 4.1. FFT Analysis of the Diffuser without Flow Control and with Typical Control of Traveling Wave Wall

FFT analysis of the unsteady fields with and without control of traveling wave wall is performed to demonstrate the validity of the simplified model. The object for FFT is the velocity across a surface, which is either placed downstream the traveling wave wall (denoted as S1 in Figure 1a) or upstream the diffuser outlet (denoted as S2 in Figure 1a).

Figure 7 shows that without the control of traveling wave wall, the frequency of 370 Hz is superior to others and signifies the natural or dominant frequency along with other discrete prominent frequencies (secondary frequencies). After introducing the first effective control of  $\tilde{f} = 1$  ( $\tilde{V} = 0.14$  and  $f_{TWW} = 370$  Hz), as shown in Figure 8, the amplitude of the dominant frequency is slightly enhanced by 1.1%, whereas many other secondary frequencies and clutters are restrained. This finding indicates that the natural frequency is enhanced and the flow field is orderly due to traveling wave wall control. The orderliness of the flow field can also be demonstrated from the vorticity contour of the flow field shown in Figures 7a and 8a.

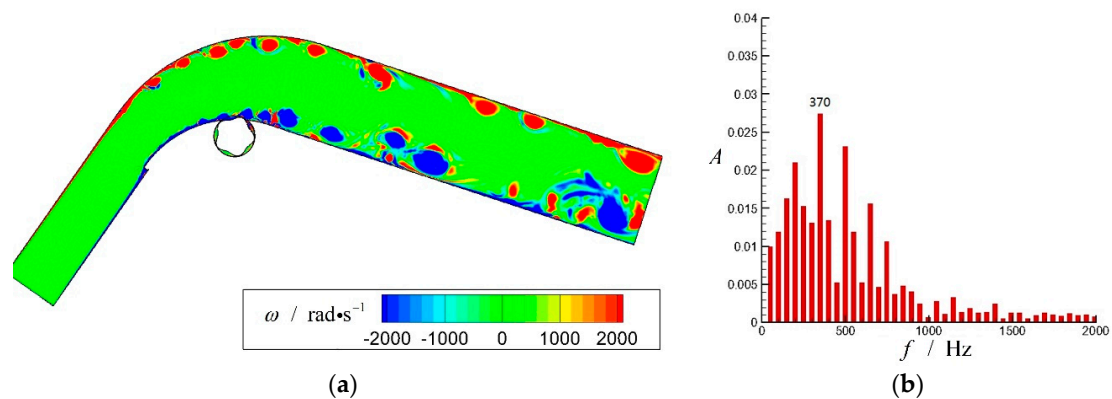


**Figure 7.** Numerical simulation of the diffuser without control ( $\tilde{V} = 0$ ,  $\tilde{f} = 0$ , and  $f_{TWW} = 0$ ): (a) Vorticity ( $\omega$ ) contour; (b) Velocity FFT of S2 ( $A - f$ ).

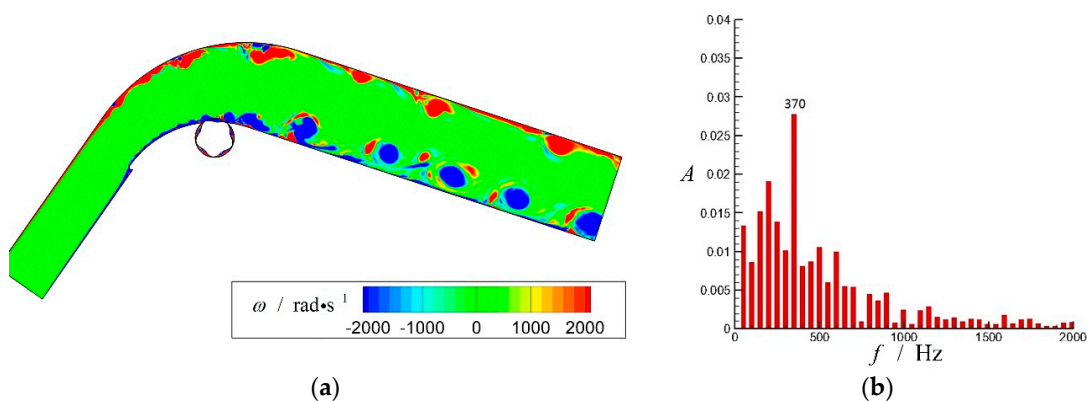


**Figure 8.** Numerical simulation of the diffuser with effective control ( $\tilde{V} = 0.14$ ,  $\tilde{f} = 1$ , and  $f_{TWW} = 370$  Hz): (a) Vorticity ( $\omega$ ) contour; (b) Velocity FFT of S2 ( $A - f$ ).

After introducing the second effective control of  $\tilde{f} = 1.5$  ( $\tilde{V} = 0.2$  and  $f_{TWW} = 540$  Hz), as shown in Figure 9, the dominant frequency is generated by the frequency of traveling wave wall (540 Hz at S1). Moreover, two vortices merge together downstream, thereby leaving only half of its frequency dominant (270 Hz at S2). However, the flow field is orderly due to one single dominant frequency of 270 Hz. As a result, the loss in the diffuser is less.

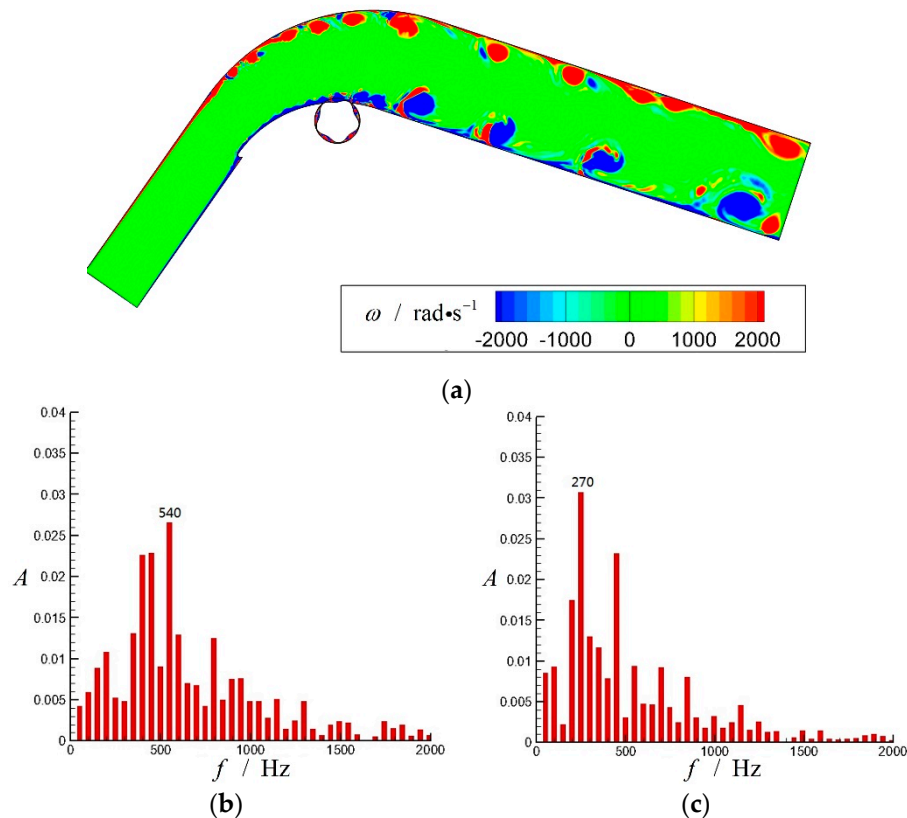


**Figure 9.** Numerical simulation of the diffuser with effective control ( $\tilde{V} = 0.2$ ,  $\tilde{f} = 1.5$ , and  $f_{TWW} = 540$  Hz): (a) Vorticity ( $\omega$ ) contour; (b) Velocity FFT of S1 ( $A - f$ ); (c) Velocity FFT of S2 ( $A - f$ ).

The same mechanism occurs when introducing the third effective control of  $\tilde{f} = 2.3$  ( $\tilde{V} = 0.3$  and  $f_{TWW} = 830$  Hz), as shown in Figure 10. However, vortices generated by the excitation of 830 Hz merge twice rather than once. Figure 10b,c shows that vortices generated by the traveling wave wall first merge from 830 Hz ones to 420 Hz ones and then merge into 210 Hz ones. Ultimately, the flow field is dominated by 210 Hz vortices. This process creates the best control effect due to energy efficiency as illustrated in Figure 3c.

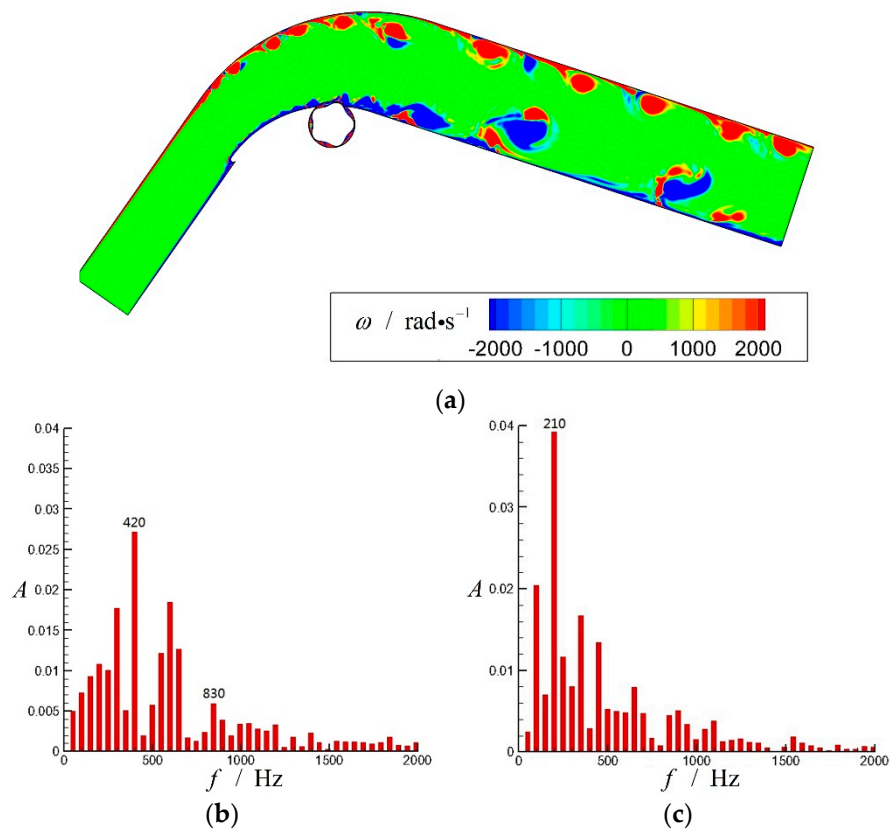


**Figure 10.** Numerical simulation of the diffuser with effective control ( $\tilde{V} = 0.3$ ,  $\tilde{f} = 2.3$ , and  $f_{TWW} = 830$  Hz): (a) Vorticity ( $\omega$ ) contour; (b) Velocity FFT of S1 ( $A - f$ ); (c) Velocity FFT of S2 ( $A - f$ ).

Invalid parameters of traveling wave wall will not generate a remarkable dominant frequency, such as those of  $\tilde{V} = 0.15$  and  $\tilde{V} = 0.28$ , as shown in Figure 11a,b.  $\tilde{V} = 0.15$  is very close to valid control of  $\tilde{V} = 0.14$ , and  $\tilde{V} = 0.28$  is twice of it. The change in natural frequency (red shift), which is also included in the simplified model, will be further explained in the following section.

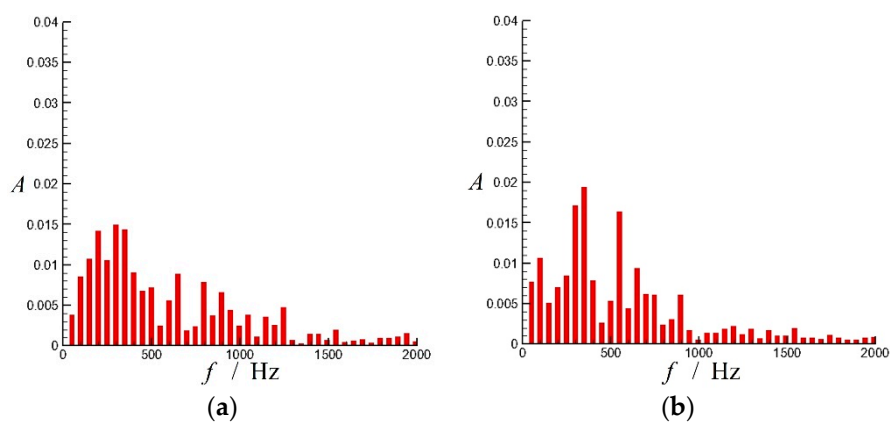


**Figure 11.** Numerical simulation of the diffuser with invalid control: (a) Velocity FFT ( $A - f$ ) of S2 ( $\tilde{V} = 0.15$ ,  $\tilde{f} = 1.04$ , and  $f_{TWW} = 380$  Hz); (b) Velocity FFT ( $A - f$ ) of S2 ( $\tilde{V} = 0.28$ ,  $\tilde{f} = 2$ , and  $f_{TWW} = 740$  Hz).

#### 4.2. Free Shear Flow Stability Interpretation

Stability theory of free shear or mixing layers is the basis for unsteady flow control [22]. Thus, in this section, the change in natural frequency and merging of vortices will be explained by free shear layers and linear stability theory.

As shown in Figure 12, the time-averaged streamwise velocity distribution  $u(y)$  downstream the separation point can be generally approximated as that of a free shear flow, which can be approximately described as

$$u(y) = \frac{U_1 + U_2}{2} + \frac{U_1 - U_2}{2} \tanh\left(\frac{y}{\delta}\right), \quad (15)$$

where  $\delta$  indicates the thickness of the mixing layer. An approximately equivalent method is used to make an analogy between a free shear flow and a real flow separation by assuming that  $U_2 \approx 0$ . This condition indicates that the phase velocity of vortex in the free shear flow equals  $U_1/2$  [22], which fits the observation in real flow separations. When  $U_1/2$  is used as the characteristic velocity  $\bar{U}$ , Equation (15) can be normalized as

$$u = 1 + \tanh\left(\frac{y}{\delta}\right), \quad (16)$$

In linear stability theory, small periodic perturbation is superposed to the basic parallel flow of mixing flow described by Equation (16). The growth rate of perturbation amplitude depends on the reduced perturbation frequency  $\tilde{\omega}$ , which is defined as

$$\tilde{\omega} = \frac{2\pi f \delta}{\bar{U}}, \quad (17)$$

where  $f$  is the frequency of the perturbation. The relationship between the growth rate of perturbation amplitude  $\alpha_i$  and  $\tilde{\omega}$ , as obtained by classic linear stability theory [23], is shown in Figure 12.  $\alpha_i$  reaches its maximum when  $\tilde{\omega} = \tilde{\omega}_m$ . Therefore,  $\tilde{\omega}_m$  is responsible for the natural or dominant frequency in the separated flow because the perturbation wave of  $\tilde{\omega}_m$  grows rapidly, such that it constitutes most of the large vortices. Thus,

$$\tilde{\omega}_m = \frac{2\pi f_n \delta}{U}, \quad (18)$$

where  $f_n$  is the local natural or dominant frequency. From the experimental study of free shear layers, an approximate relation can be obtained as [24]

$$\delta \approx \delta_0 + kx, \quad (19)$$

where  $\delta_0$  is the initial thickness of shear layer,  $x$  is the distance downstream the starting point of shear layer, and  $k$  is a coefficient. Thus,  $\delta$  increases downstream because large amounts of momentum are transferred from the high velocity mainstream to the low velocity one. Considering the lack of characteristic length in free shear layer,  $\delta$  grows without limit. However, in an actual flow separation such as in a curved diffuser, equivalent  $\delta$  is limited because of the characteristic length, such as the existing length of the separation zone. Thus, an approximate relation imitating the free shear flow is used as follows:

$$\begin{cases} \delta \approx \delta_0 + kx & 0 < x < x_c \\ \delta \approx \delta_0 + kx_c & x_c < x \end{cases}, \quad (20)$$

where  $\delta$  indicates the equivalent thickness of mixing layer in the flow separation after the separation point,  $x$  indicates the distance downstream the separation point, and  $x_c$  indicates the position where  $\delta$  does not grow. Using this relation combined with Equation (18), the local natural frequency for a flow separation with scale limit can be described as

$$\begin{cases} f_n \approx \frac{U\tilde{\omega}_m}{2\pi(\delta_0+kx)} & 0 < x < x_c \\ f_n \approx \frac{U\tilde{\omega}_m}{2\pi(\delta_0+kx_c)} & x_c < x \end{cases}. \quad (21)$$

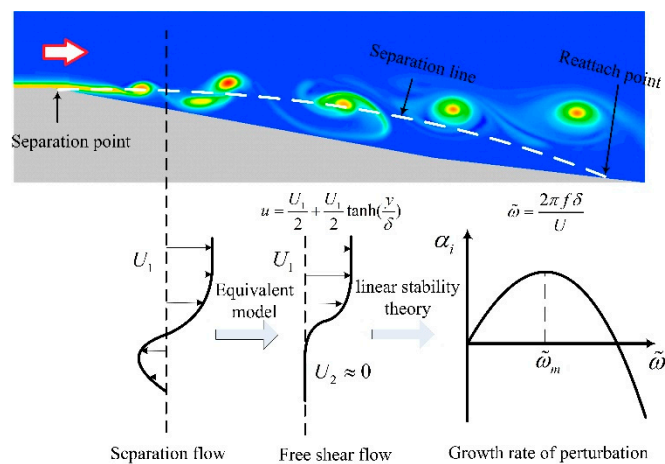


**Figure 12.** Relationship between flow separations and free shear layers based on linear stability theory.

Equation (21) indicates that the natural frequency can be regarded as the dominant frequency after  $x_c$ , which is  $U\tilde{\omega}_m/2\pi(\delta_0 + kx_c)$ . Moreover, the change in natural frequency and merging of vortices are extremely related to and can be explained by the theory above. The velocity distribution of a flow separation is equivalent to that of a free shear layer in Figure 12. Velocity distributions of all free shear layers are analogous, which indicates that they share the same  $\tilde{\omega}_m$ . For a determined  $\tilde{\omega}_m$ , the increase in phase velocity of the traveling wave wall promotes the momentum transfer from the mainstream to the separation zone, which in turn increases  $\delta_0$ . As a result,  $f_n$  decreases, as indicated in Equation (21), under the condition that  $x_c < x$ . Thus, the increase in non-dimensional frequency of traveling wave wall reduces the natural frequency, which is in turn responsible for the decrease in the natural frequency in the flow field. When mixing develops downstream, as indicated by the increase in  $x$ ,  $f_n$  also decreases in accordance with Equation (21) under the condition that  $0 < x < x_c$ . For example, as  $x$  increases,  $\delta$  increases to  $2\delta$ . As a result, the local dominant frequency  $f_n$  decreases to  $f_n/2$ . This condition physically implies that the two vortices of frequency  $f_n$  merge and compose a large vortex of its half frequency  $f_n/2$ . The merging of vortices causes the phenomenon shown in Figures 9 and 10, which provide a new insight for effective control when excitation frequency is some integral multiple of the natural frequency.

#### 4.3. Mechanism Analysis of Flow Control Using Traveling Wave Wall

The phenomena of traveling wave control are due to three mechanisms: unitary orderliness of frequency vortices, red shift of natural frequency, and merging of vortices. The red shift of natural frequency and merging of vortices are discussed in detailed in the last section, while the former has already been introduced in the simplified model. The two mechanisms are demonstrated by FFT analysis. The unitary orderliness of frequency vortices will make the flow field orderly and reduce the flow loss. This mechanism is introduced in the simplified model and demonstrated by FFT analysis.

A brief method is used to explain the phenomena shown in Figure 3, in consideration of the three mechanisms above. As the phase velocity of the traveling wave increases, the reduced frequency of traveling wave increases, whereas the natural frequency decreases due to instability (when  $x_c < x$ ). This trend is shown as the heavy line in Figure 13. This line is nearly constant when the reduced frequency is low and drops slowly when the reduced frequency is very high. The reason is two-fold: one is that the low phase velocity slightly affects the natural frequency, and the other is that very high phase velocity acts more similarly to a smooth cylinder than a traveling wave wall. When the natural frequency is enhanced, the unitary orderliness of frequency vortices makes the flow field orderly and reduces flow loss. Thus, a good effect point from the traveling wave wall must lie on the line  $\tilde{f}_n = \tilde{f}$ , which is reflected as a fine line in Figure 13. However, the merging of vortices ( $0 < x < x_c$ ) results in that external excitations of two, four, or more times the natural frequency will have good

control effects due to the merging of vortices once, twice, or more. In Figure 13, this mechanism is reflected by fine lines identified by  $2\tilde{f}_n = \tilde{f}$  and  $4\tilde{f}_n = \tilde{f}$ . The numerical results in Figure 13 show that the intersection points of the heavy line and fine lines have the reduced control frequencies of 1, 1.5, and 2.3. This finding explains the peculiar phenomenon in Figure 3.

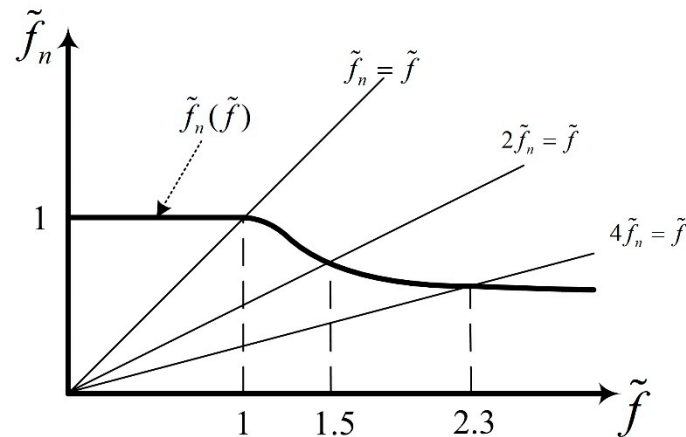


**Figure 13.** Relationship between the reduced natural frequency  $\tilde{f}_n$  and the reduced control frequency  $\tilde{f}$ .

In summary, the phenomena of the traveling wave control effect (as illustrated in Figure 3) are explained using the simplified model, FFT analysis, and linear stability theory of free shear layers. Specifically, these phenomena are due to three mechanisms: unitary orderliness of frequency vortices, red shift of the natural frequency, and merging of vortices. Traveling wave wall with increased phase velocity promotes momentum transfer from the mainstream to the separation zone, which changes the natural frequency of the separation flow. External excitation can strengthen the dominated frequency of the K–H wave, which in turn forms the large-scale unstable vortices and restrains the small-scale vortices. As a result, the flow field becomes orderly and less chaotic. Ultimately, the flow loss decreases. The merging of vortices will generate frequencies of two or four times the natural frequency, thereby resulting in discrete frequencies of good control effect.

## 5. Conclusions

Traveling wave wall is a useful method to suppress flow separations. In this study, rigid traveling wave wall control in a diffuser is investigated by numerical simulation. The results show that the flow control effects under the discrete phase velocities or frequencies of the traveling wave wall are better than those under the adjacent frequencies. To explain this phenomenon, a Duffing-based nonlinear simplified model of flow separations with unsteady flow control is used. The characteristics of the model are then investigated to describe the obtained trends. Detailed information is drawn from the numerical results through FFT analysis. The spectra show three mechanisms: unitary orderliness of frequency vortices, red shift of the natural frequency, and merging of vortices, some of which are also explained theoretically by linear stability theory. The main conclusions are obtained as follows:

- (1) Numerical simulation of a diffuser controlled by a rigid traveling wave wall is performed, and a parameter named energy efficiency is defined to evaluate the control effect. In this case, energy efficiency increases first and then decreases as the phase velocity or the reduced frequency of the traveling wave wall increases. However, three discrete reduced frequencies of 1, 1.5, and 2.3 have better control effect than the adjacent frequencies, and the corresponding relative total pressure loss coefficients are about  $-10\%$ ,  $-15\%$ , and  $-18\%$ , respectively. This property serves as a unique characteristic of traveling wave wall control. Also, the maximum energy efficiency is about 50, which means the traveling wave wall control is very economical. Both of the high effectiveness and economy indicate the engineering practicability of traveling wave wall controls.

- (2) Duffing-based nonlinear simplified model for traveling wave wall control is used. The interaction of the traveling wave wall to this dynamic system is modeled as a periodic external excitation and the change in natural frequency. External periodic excitation, which imitates the form of a K–H wave, is added into the model. Thus, the complete nondimensional form of the model can be stated as:

$$\frac{d^2y}{dt^2} = y - 4y^3 - K\frac{dy}{dt} + A \sin(1.1t) + A_e \sin(1.1\frac{\omega_e}{k}t)$$

- (3) With a given  $k$ , which is a function of reduced frequency, the characteristic of the simplified model is obtained using MLE. MLE is considerably decreased when the reduced frequencies equal 1, 1.6, and 2.1. This case indicates high orderliness compared that of adjacent frequencies. This deduction is supported by the time–displacement and velocity–displacement phase diagrams and FFT analysis of displacement. Furthermore, the same phenomenon in the numerical simulation reflects that the nonlinear model can effectively explain the behavior of such chaotic flows.
- (4) FFT analysis of numerical simulation proves the red shift of natural frequency and merging of vortices, which are also theoretically explained by linear stability theory of free shear layers.
- (5) Using numerical simulation, a simplified nonlinear model, FFT analysis, and linear stability theory, three mechanisms are found responsible for the peculiar phenomena in traveling wave wall control: unitary orderliness of frequency, red shift of the natural frequency, and merging of vortices. Therefore, as phase velocity increases, natural frequency drops continuously. The merging of vortices results in that the reduced frequency is one, two, or four times the natural frequency. This condition will strengthen the dominant separation vortices and make the flow field orderly, thereby resulting in good control effect.

**Author Contributions:** W.L. performed the data analyses and wrote the manuscript; G.H. proposed the conception of the study; J.W. and Y.Y. contributed to simulation and manuscript preparation.

**Funding:** This research was funded by the National Basic Research Program of China (No. 2014CB239602) and the National Natural Science Foundation of China (No. 51176072).

**Acknowledgments:** The authors wish to express their gratitude to Jiangsu Province Key Laboratory of Aerospace Power System (affiliated with the College of Energy and Power Engineering, Nanjing University of Aeronautics and Astronautics) for technical support. The team members of College of Energy and Power Engineering of Nanjing University of Aeronautics and Astronautics are also gratefully acknowledged for their cooperation.

**Conflicts of Interest:** The authors declare no conflict of interest.

## References

- Hertel, H. *Structure Form Movement*; Reinhold: New York, NY, USA, 1966.
- Choi, K.S. *Emerging Techniques in Drag Reduction*; John Wiley & Sons: London, UK, 1996.
- Wu, C.J.; Wang, L.; Wu, J.Z. Suppression of the Von Karman Vortex Street Behind a Circular Cylinder by a traveling Wave Generated by a Flexible Surface. *J. Fluid Mech.* **2007**, *574*, 365–391. [[CrossRef](#)]
- Wu, C.J.; Xie, Y.Q.; Wu, J.Z. “Fluid Roller Bearing” Effect and Flow Control. *Acta Mech. Sin.* **2003**, *19*, 476–484.
- Wu, J.M.; Wu, J.Z.; Wu, C.J.; Vakili, A.D. Preliminary Study of Nonlinear Flow over Traveling Wavy Wall. *Int. Symp. Nonsteady Fluid Dyn.* **1990**, *92*, 359–368.
- Wu, J.Z.; Wu, J.M. Vorticity Dynamics on Boundaries. *Adv. Appl. Mech.* **1996**, *32*, 119–275.
- Yang, Z.; Wu, J.Z. Drag Reduction by Axisymmetric Traveling Wavy Wall. *J. Univ. Sci. Technol. China* **2005**, *35*, 471–479.
- Wu, Q.Y. Study on Numerical Simulation of Active Control by Using Traveling Wave Wall of Flow Around a Circular Cylinder. Master’s Thesis, Harbin Institute of Technology, Harbin, China, 2013; pp. 37–38. (In Chinese)
- Chen, W.; Liu, Y.; Hu, H. Suppression of Vortex Shedding from a Circular Cylinder by using a Traveling Wave Wall. In Proceedings of the 52nd Aerospace Sciences Meeting, National Harbor, MD, USA, 13–17 January 2014. AIAA 2014-0399.

10. Zheng, X.Q.; Zhou, X.B.; Zhou, S. Investigation on a type of flow control to weaken unsteady separated flows by unsteady excitation in axial flow compressors. *J. Turbomach.* **2005**, *127*, 489–496. [[CrossRef](#)]
11. Greenblatt, D.; Wygnanski, I.J. The Control of Flow Separation by Periodic Excitation. *Prog. Aerosp. Sci.* **2000**, *36*, 487–545. [[CrossRef](#)]
12. Chatterjee, A. An introduction to the proper orthogonal decomposition. *Curr. Sci.* **2000**, *78*, 809–817.
13. Lumley, J.L. The Structure of Inhomogeneous Turbulent Flows. In *Atmospheric Turbulence and Radio Wave Propagation*; Nauka: Moscow, Russian, 1967; pp. 166–178.
14. Vinuesa, R. *Synergetic Computational and Experimental Studies of Wall-Bounded Turbulent Flows and Their Two-Dimensionality*; Illinois Institute of Technology: Chicago, IL, USA, 2013.
15. Qi, L.; Zou, Z.; Wang, P.; Cao, T.; Liu, H. Control of secondary flow loss in turbine cascade by streamwise vortex. *Comput. Fluids* **2012**, *54*, 45–55. [[CrossRef](#)]
16. Batchelor, G.K. *An Introduction to Fluid Dynamics*; Cambridge University Press: Cambridge, UK, 1967.
17. Kovacic, I.; Brennan, M.J. *The Duffing Equation: Nonlinear Oscillators and Their Behavior*; John Wiley & Sons: Hoboken, NJ, USA, 2011.
18. Huang, G.; Lu, W.; Zhu, J.; Fu, X.; Wang, J. A nonlinear dynamic model for unsteady separated flow control and its mechanism analysis. *J. Fluid Mech.* **2017**, *826*, 942–974. [[CrossRef](#)]
19. Zhuang, L.X.; Yi, X.Y.; Ma, H.Y. *Fluid Mechanics*, 2nd ed.; Press of University of Science and Technology of China: Hefei, China, 2012.
20. Benettin, G.; Galgani, L.; Giorgilli, A.; Strelcyn, J.M. Lyapunov characteristic exponents for smooth dynamical systems; a method for computing all of them: Part I: Theory, Part II: Numerical applications. *Meccanica* **1980**, *15*, 9–20. [[CrossRef](#)]
21. Lorenz, E.N. Deterministic non periodic flow. *J. Atmos. Sci.* **1963**, *20*, 130–141. [[CrossRef](#)]
22. Stuart, J.T. On finite amplitude oscillations in laminar mixing layers. *J. Fluid Mech.* **1967**, *29*, 417–440. [[CrossRef](#)]
23. Drazin, P.C. *Hydrodynamic Stability*, 2nd ed.; Cambridge Mathematical Library: Cambridge, UK, 2012.
24. Oster, D.; Wygnanski, I. The forced mixing layer between parallel streams. *J. Fluid Mech.* **1982**, *123*, 91–130. [[CrossRef](#)]



© 2019 by the authors. Licensee MDPI, Basel, Switzerland. This article is an open access article distributed under the terms and conditions of the Creative Commons Attribution (CC BY) license (<http://creativecommons.org/licenses/by/4.0/>).